Theoretical and experimental studies on the electronic structure of crystalline and amorphous $ZnSnO_3$ thin films

Joohwi Lee,[1,2] Deok-Yong Cho,[3] Jisim Jung,[2] Un Ki Kim,[2] Sang Ho Rha,[2] Cheol Seong Hwang,[2] and Jung-Hae Choi[1,a)]

[1]*Electronic Materials Research Center, Korea Institute of Science and Technology, Seoul 136-791, South Korea*
[2]*WCU Hybrid Materials Program, Department of Materials Science and Engineering, and Inter-University Semiconductor Research Center, Seoul National University, Seoul 151-744, South Korea*
[3]*CFI-CES, Institute for Basic Science, and Department of Physics and Astronomy, Seoul National University, Seoul 151-747, South Korea*

(Received 4 April 2013; accepted 6 June 2013; published online 20 June 2013)

The influence of structural disorder on the electronic structure of amorphous $ZnSnO_3$ was examined by *ab-initio* calculations. The calculation results are compared with the experimental results using as-deposited and annealed $ZnSnO_3$ films grown by atomic layer deposition. The O K-edge X-ray absorption spectroscopy, X-ray diffraction, and thin-film transistors were employed in the experiment. The conduction band minima of amorphous and crystalline $ZnSnO_3$ mainly consisted of Sn 5s state, while a higher non-uniform localization of these states was observed in the amorphous phase compared with the crystalline counterpart. The experimental results coincide well with the theoretical results. © *2013 AIP Publishing LLC*. [http://dx.doi.org/10.1063/1.4811788]

Amorphous oxide semiconductor (AOS) is a crucially important class of material for several next-generation electronic devices. Among them, thin-film transistors (TFTs) are important for high-performance electronic display[1,2] and memory[3] applications. The conventional amorphous Si and polycrystalline Si used as the channel layer in TFTs have problems with low carrier mobility ($\ll 1\,cm^2/V\,s$) and the presence of grain boundaries, respectively. In contrast, several AOSs have intriguing properties when used as the channel layer, such as high electron mobility ($>10\,cm^2/V\,s$) across a wide composition range, structural stability in an extensive temperature range, and easy fabrication even at room temperature. $InGaZnO_x$ (IGZO) is perhaps the most well-known AOS in these regards,[4] and display devices with IGZO-channel TFTs are already commercially available.[5] The electrical properties of IGZO are mainly ascribed to its peculiar electronic structure near the conduction band edge, which is mainly composed of In 5s orbitals.[6] The strong delocalization of the In 5s orbital features near the conduction band minimum (CBM), even in amorphous structure, contributes to the high electron mobility.[7] However, In is expensive, and the low binding energy of In with oxygen sometimes brings about concerns with reliability.[8]

Therefore, an alternative AOS material not containing In is necessary for further development. Materials comprising ZnO and SnO_2 are interesting in this regard, since many of them show favorable electrical properties for use as the channel in TFTs, while maintaining amorphous structure.[1,9–11] Among them, $ZnSnO_3$ (ZTO) is a highly promising material due to its high mobility and easy fabrication.[1] However, $ZnSnO_3$ is thermodynamically less stable compared with ($Zn_2SnO_4 + SnO_2$),[12,13] so detailed studies on its electronic band structures and accompanied properties have been limited. Particularly, detailed comparative studies on the theoretical aspects of the electronic structures of the crystalline and amorphous ZTO materials are still lacking, despite their importance. Therefore, in this study, the detailed electronic structures of crystalline and amorphous phases of ZTO were theoretically examined based on *ab-initio* calculations, and the results were compared with the experimental results using ZTO films deposited by atomic layer deposition (ALD). The change in the atomic structures of the ZTO thin films was examined by various structural and electrical characterization methods. The O K-edge X-ray absorption spectroscopy (XAS) was used to directly compare the experimental and theoretical electronic structures of amorphous and nano-crystalline ZTO films.

Ab-initio calculations based on density functional theory implemented in VASP code[14,15] were performed. Amorphous phases were obtained from *ab-initio* molecular dynamic simulations with melt-quenching method and soft O pseudo-potential at the Γ-point. The randomizing and melting were performed at 5000 K and 2500 K for 1 ps and 10 ps, respectively. Quenching was performed with a rate of 50 K/ps. It was confirmed that no peroxide bonds (O-O) were formed by fast quenching.[7] Hexagonal supercell-cell was employed for crystalline lithium niobate phase,[12] which was reported to be thermodynamically more stable than the ilmenite phase,[16] and pseudo-cubic super-cells were employed for the amorphous phase. One hundred and twenty atoms (72 O, 24 Sn, 24 Zn) were included for both calculations. The optimizations of super-cells were performed with the full relaxations of atomic positions and eliminating the external pressures using the generalized gradient approximations corrected for on-site Coulombic interactions[17] (GGA + U) on the Perdew–Burke–Ernzerhof functional[18] with $4 \times 4 \times 4$ Γ-centered *k*-space sampling. Effective U values of 7.5 eV for Zn and 3.5 eV for Sn were selected by referring to previous reports on binary oxides.[19,20] The energies and volumes for super-cells with five different amorphous phases were well converged, within deviations of 0.07 eV per formular unit

a)Author to whom correspondence should be addressed. Electronic mail: choijh@kist.re.kr

0003-6951/2013/102(24)/242111/5/$30.00 © 2013 AIP Publishing LLC

(f.u.) and 4%, respectively. The energies of amorphous super-cells are about 0.6 ~ 0.75 eV/f.u. higher than that of crystalline super-cell and the values are reasonable compared with previous calculations reports of other AOSs.[7] The most energetically stable super-cell was chosen to show the electronic structures of amorphous ZTO. Projected density of states (PDOSs) was obtained using a Gaussian smearing of 0.05 eV.

In order to examine the disorder effects in ZTO experimentally, two 60-nm-thick ZTO thin films were prepared by ALD using $C_4H_{10}Zn$, $C_{12}H_{28}N_2O_2Sn$, and O_3 as the precursors for Zn, Sn, and O, respectively, on a Si wafer at 150 °C. The ALD deposition cycles of ZnO and SnO_2 comprised steps of Zn (Sn) source injection, purge, O_3 injection, and purge, for 1 (2), 10 (5), 3 (5), and 10 s, respectively, which were optimized for each component oxide. For achieving a Zn:Sn composition of 1:1, one ZnO deposition and three Sn deposition cycles were employed. The film composition (Zn:Sn ratio) was estimated by X-ray fluorescence spectroscopy. One of the samples was annealed at 600 °C for 1 h in air atmosphere to compare the structural changes with those of the as-deposited sample. There is no change in the Zn:Sn ratio during the annealing. X-ray diffraction (XRD, PANalytical, X'pert Pro) and XAS were employed to examine the structural changes in the film by the annealing. The O K-edge XAS was performed in 2A beamline at the Pohang Light Source, where the energy resolution of the X-rays was approximately 0.2 eV. Atomic force microscopy (AFM, JEOL JSPM-5200) was used to confirm the surface morphologies, and the electrical properties of the as-deposited and annealed ZTO films were examined by fabricating TFT structures on SiO_2 (gate dielectric layer)/heavily-doped p-type Si (gate) wafers. Ti was used as the source and drain contact metal. The channel layer was patterned by HF solution, and the channel length and width were 100 and 65 μm, respectively.

The left panel in Fig. 1 shows the (a) total DOS (TDOS), and the (b) O, (c) Sn, and (d) Zn PDOSs for the crystalline phase. The CBM was referenced as zero energy (vertical dashed lines). The features are assigned as A-H by orbital characters. Feature A is mainly attributed to the Sn 4d orbital, which is weakly hybridized with the O 2s orbital. Feature B is for the O 2s state hybridized with the metal orbitals, feature C is for the Zn 3d state, and features D and E represent the valence band (VB), which is mainly composed of O 2p orbitals. The Zn 3d orbitals are strongly hybridized with the O 2p states, so as to spread out in the VB, and even contribute to the VB maximum (VBM). Feature F is for near the CBM, which is mostly contributed by Sn 5s–O 2p. On the other hand, the higher-energy-state features G and H are attributed to Zn 4s–O 2p and Zn 4p/Sn 5p–O 2p hybridized states. The direct bandgap was estimated to be about 2.4 eV. The underestimated bandgap compared with the experimental value reported for transparent oxides (>3 eV) could be attributed to the incomplete cancellation of the self-interaction term from the density functional approximation.[21]

These calculation results reveal that the Sn 5s states near the CBM have a major influence over the electrical conduction behavior of the fabricated TFT. Therefore, these states require attention. The degree of localization of the DOS, particularly near the CBM, has a crucial influence on the electron carrier transport under an electric field. To measure the degree of the localization of the DOSs, an inverse participation ratio (IPR) was analyzed, as shown in Fig. 1(e). IPR is defined as follows:

$$IPR = \frac{\sum_i |a_i|^4}{\left(\sum_i |a_i|^2\right)^2}, \quad (1)$$

where a_i denotes the projected wave function on each atomic site i. IPR is related to the uniformity of the distribution of the wave functions, with a higher value indicating a predominance of PDOSs at a specific site.[22] The IPR values are rather uniform throughout the valence band and conduction band, except for the Zn 3d and Sn 4d (features A and C). This indicates that the electrical conduction in crystalline ZTO is uniformly contributed by all the atomic sites.

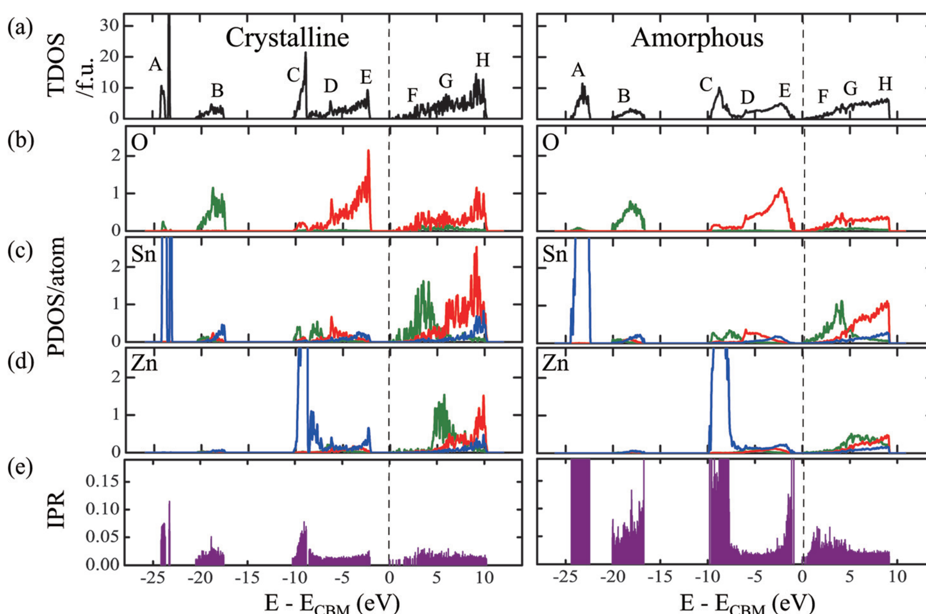

FIG. 1. (a) TDOS (b) PDOSs of O, (c) Sn, and (d) Zn. Conduction bands are three times multiplied for better viewing. (e) IPR for the crystalline (left panel) and amorphous (right panel) ZTO.

TABLE I. CNs and bond lengths of metal-O for crystalline and amorphous ZTO.

	Crystalline		Amorphous	
	CN	Bond lengths (Å)	CN	Bond length (Å)
Zn (-O)	6	$3 \times 1.97, 3 \times 2.29$	4.28 ± 0.14[a]	1.98 ± 0.11[b]
Sn (-O)	6	$3 \times 2.03, 3 \times 2.06$	5.70 ± 0.02[a]	2.06 ± 0.08[b]

[a]The CN was measured for each amorphous super-cell and the average and standard deviation obtained from five different amorphous super-cells are shown here.

[b]The bond lengths were collected from the five different amorphous super-cells and the average and standard deviation are shown here.

The right panel of Fig. 1 shows (a) the TDOS and the (b) O, (c) Sn, and (d) Zn PDOSs for the amorphous ZTO phase. Compared with the crystalline phase, the overall features are smeared, which was probably due to the structural disorders. The direct bandgap was estimated to be 1.2 eV, which is much smaller than the value of crystalline phase (2.4 eV). This is mainly attributed to the tailing of the VB states that can also be detected in experiments.[23] The IPR values for the amorphous phase are more complicated, as shown in Fig. 1(e). Most of IPR values increased except the mid-range of VB and CB (features D and G). Note that the IPR values for the features near the VBM and CBM (features E and F) are certainly increased compared with the crystalline phase. This clearly shows that the states near the CBM/VBM are concentrated at certain specific atomic sites. Therefore, the Zn 3d–O 2p VB and the Sn 5s CB in the amorphous phase are more localized than those in the crystalline phase.

Table I shows the coordination numbers (CN) of metals and the average bond length of metal-O bonds. The cutoff lengths of metal-O bonds were selected as the first minima from a radial distribution function. The CN of Zn decreased from six in the crystalline phase to around four in the amorphous phase. Considering the preference of tetrahedral sites of a Zn atom, disorder effects may weaken the interactions of Zn-O by Sn. The bond length also decreased to be close to that of binary oxide. The decrease in both the CN of Zn and the bond length of Zn-O by amorphization was found in other AOS materials, such as IGZO and $InZnSnO_x$ by extended X-ray absorption fine structure.[6,24] This means that the orbital overlap of O 2p-Zn 4s increases, and the O 2p-Sn 5s hybridization is relatively reduced in the amorphous phase, which results in less uniform delocalization of the Sn 5s states.

Details about the CB electronic structures of crystalline and amorphous materials are shown in Fig. 2(a). In the crystalline phase, the intensity of the Sn 5s PDOS is comparable with that of the Zn 4s PDOS, while in the amorphous phase, the intensity of the Sn 5s PDOS far exceeds that of the Zn 4s PDOS. The decrease in Zn 4s PDOS can be understood as a consequence of structural disorders in the Zn sites due to amorphization. Longer tails of the Zn 4s state toward the CBM might increase the O 2p PDOS below + 4 eV due to Zn 4s-O 2p hybridization facilitating Zn-O hopping interactions. Meanwhile, Sn 5s PDOS does not decrease in intensity, but becomes sharp with narrow peak features near +4 eV in the case of the amorphous phase. The ratio of [Sn 5s PDOS] / [O 2p PDOS] increases, and the ratio would increase further if the contribution of the Zn 4s hybridization is subtracted from the O 2p PDOS. This effect increased the effective mass of Sn 5s and reduced the hybridization strength, which suggests a selective localization of the Sn 5s CB in the case of amorphous ZTO.

Fig. 2(b) shows the partial charge densities for CBM for crystalline (left) and amorphous (right) ZTO and more directly shows the selective localization in the amorphous phase. The CBM mainly formed by Sn 5s and O 2p shows uniform hybridization and delocalization to all of the spaces in crystalline ZTO. However, the partial charge densities of CBM are not uniform for the whole Sn 5s in amorphous ZTO. In this case, the electron transfer path of Sn $\rightarrow$ O $\rightarrow$ Sn would be spatially limited compared with the crystalline structure.

Fig. 3 shows the structural and electrical characteristics of the as-deposited and annealed ZTO films. The XRD spectra in Fig. 3(a) show that the as-deposited film has a completely amorphous structure, while the annealed film has a more ordered structure due to the transformation into the nano-crystalline structure (slight bump feature at 2θ value of about $30° \sim 32°$). The AFM images in Fig. 3(b) showed that the annealed film have a slightly grainy microstructure compared with the as-deposited film, corroborating the nano-crystallization. The electrical test using TFT structure indicated that the as-deposited film was too insulating to show any reasonable TFT operation, suggesting a very low carrier density and effective mobility. However, the annealed ZTO

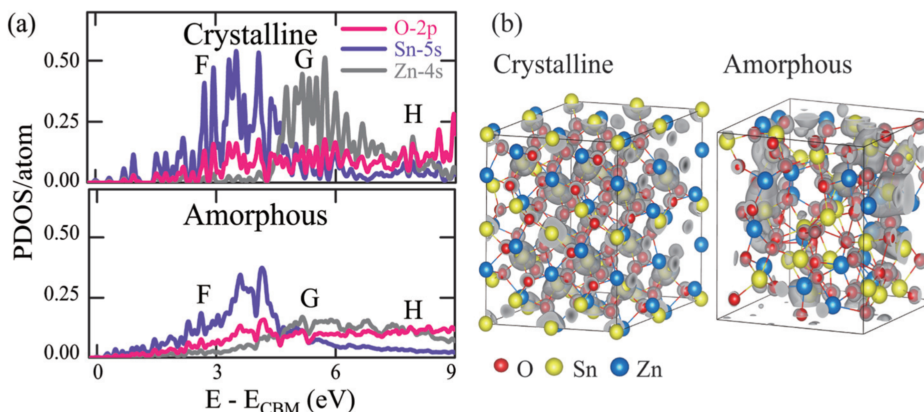

FIG. 2. (a) PDOSs of the conduction band region for crystalline (upper) and amorphous (lower) ZTO. (b) Partial charge densities of CBM for crystalline (left) and amorphous (right) ZTO. Isosurface level is 0.0005 electrons/$Å^3$.

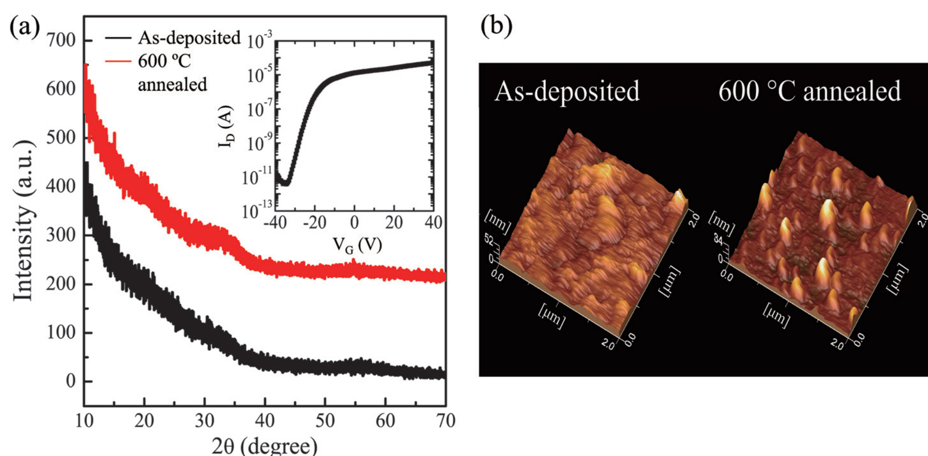

FIG. 3. (a) XRD spectra for as-deposited and 600 °C annealed ZTO films. Inset shows the drain current (I_D) vs. gate voltage (V_G) curve of a TFT using the ZTO film annealed at 600 °C. (b) AFM images for as-deposited ZTO film and that annealed at 600 °C.

film showed an n-type conductivity that is high enough for reasonable TFT behavior (drain current vs. gate voltage) as shown in the inset of Fig. 3(a). The calculated saturation mobility was ~1.5 cm^2/V s, which is quite low compared with the sputtered film.[10] Nevertheless, the annealing certainly increased the carrier mobility from a negligible level to a measurable level. The increased mobility of the annealed film can be understood from the nano-crystalline structure of the material, of which the electron mobility near CBM must be higher than that of the as-deposited amorphous material, as can be understood from the more delocalized nature of Sn 5s PDOS in the theoretical calculation. In addition, it was also reported that thermal annealing improved the mobility of device, even for the different compositions of ALD ZTO films (Zn: Sn = 2.5: 1).[11]

Fig. 4 shows the O K-edge XAS spectra of the as-deposited and annealed ZTO thin films. The features in the unoccupied band structures (F-H) are well reproduced in the experimental XAS. Compared with the annealed sample, the as-deposited sample has a stronger feature F. The higher peak intensity can be interpreted as a signature of strong Sn 5s localization in the as-deposited sample, since O K-edge XAS reflects the unoccupied PDOS of the metal ions that hybridize with the O 2p orbital states through the O 1s → 2p dipole transition. These experimental findings are consistent with the calculation results based on *ab-initio* calculations.

In summary, the electronic structure of crystalline and amorphous ZTO phases have been examined by *ab-initio* theoretical study, and the results were experimentally confirmed by XAS. It was concluded that the orbital character of the lowest CB was mostly Sn 5s for both phases. However, the CB state was more localized for amorphous structure compared with the crystalline case, although the degree of localization was not significant. Structural characterization and electrical tests of the as-deposited and annealed ALD ZTO films showed good agreement between the theoretical estimation and experiment. The ZTO film was nano-crystallized (or just slightly more ordered only in a short range), even after the annealing at 600 °C, and possessed enhanced electrical properties, which renders ZTO an important channel material for high-performance TFTs.

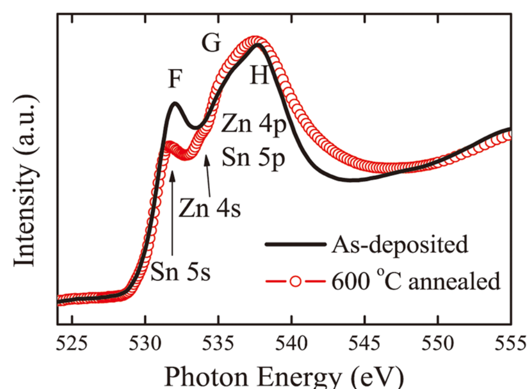

FIG. 4. O K-edge XAS for as-deposited ZTO film and that annealed at 600 °C.

This work was supported by the IT R&D program of MKE/KEIT (10035320, Development of Novel 3D Stacked Device and Core Materials for the Next Generation Flash Memory) and by the Converging Research Center Program through the MEST (2012K001300). Experiment at the PLS was supported in part by the MEST and POSTECH. The authors appreciate the fruitful advice on the amorphous model from Mr. Youngho Kang and Professor Seungwu Han in Seoul National University.

[1]P. Görrn, M. Sanders, J. Meyer, M. Kröger, E. Becker, H.-H. Johannes, W. Kowalsky, and T. Riedl, Adv. Mater. **18**, 738 (2006).
[2]T. Kamiya and H. Hosono, NPG Asia Mater. **2**, 15 (2010).
[3]S. H. Rha, J. Jung, Y. S. Jung, Y. J. Chung, U. K. Kim, E. S. Hwang, B. K. Park, T. J. Park, J.-H. Choi, and C. S. Hwang, Appl. Phys. Lett. **100**, 203510 (2012).
[4]K. Nomura, H. Ohta, A. Takagi, T. Kamiya, M. Hirano, and H. Hosono, Nature **432**, 488 (2004).
[5]S. Eguchi, H. Shinoda, T. Isa, H. Miyake, S. Kawashima, M. Takahashi, Y. Hirakata, S. Yamazaki, M. Katayama, K. Okazaki, A. Nakamura, K. Kikuchi, M. Niboshi, Y. Tsukamoto, and S. Mitsui, SID Int. Symp. Digest Tech. Paper **43**, 367 (2012).
[6]D.-Y. Cho, J. Song, K. D. Na, C. S. Hwang, J. H. Jeong, J. K. Jeong, and Y.-G. Mo, Appl. Phys. Lett. **94**, 112112 (2009).
[7]A. Walsh, J. L. F. Da Silva, and S.-H. Wei, Chem. Mater. **21**, 5119 (2009).
[8]H.-H. Nahm, Y.-S. Kim, and D. H. Kim, Phys. Status Solidi B **249**, 1277 (2012).
[9]H. Q. Chiang, J. F. Wager, R. L. Hoffman, J. Jeong, and D. A. Keszler, Appl. Phys. Lett. **86**, 013503 (2005).
[10]B. S. Yang, S. Park, S. Oh, Y. J. Kim, J. K. Jeong, C. S. Hwang, and H. J. Kim, J. Mater. Chem. **22**, 10994 (2012).
[11]J. Heo, S. B. Kim, and R. G. Gordon, Appl. Phys. Lett. **101**, 113507 (2012).
[12]Y. Inaguma, M. Yoshida, and T. Katsumata, J. Am. Chem. Soc. **130**, 6704 (2008).
[13]H. Gou, J. Zhang, Z. Li, G. Wang, F. Gao, R. C. Ewing, and J. Lian, Appl. Phys. Lett. **98**, 091914 (2011).

[14]G. Kresse and J. Furthmüller, Phys. Rev. B **54**, 11169 (1996).
[15]G. Kresse and J. Furthmüller, Comput. Mater. Sci. **6**, 15 (1996).
[16]D. Kovacheva and K. Petrov, Solid State Ionics **109**, 327 (1998).
[17]S. L. Dudarev, G. A. Botton, S. Y. Savrasov, C. J. Humphreys, and A. P. Sutton, Phys. Rev. B **57**, 1505 (1998).
[18]J. P. Perdew, K. Burke, and M. Ernzerhof, Phys. Rev. Lett. **77**, 3865 (1996).
[19]F. Oba, M. Choi, A. Togo, A. Seko, and I. Tanaka, J. Phys. Condens. Matter **22**, 384211 (2010).
[20]A. K. Singh, A. Janotti, M. Scheffler, and C. G. Van de walle, Phys. Rev. Lett. **101**, 055502 (2008).
[21]R. A. Heaton, J. G. Harrison, and C. C. Lin, Phys. Rev. B **28**, 5992 (1983).
[22]E. Cho, S. Han, D. Kim, H. Horii, and H.-S. Nam, J. Appl. Phys. **109**, 043705 (2011).
[23]P. T. Erslev, E. S. Sundholm, R. E. Presley, D. Hong, J. F. Wager, and J. D. Cohen, Appl. Phys. Lett. **95**, 192115 (2009).
[24]C. A. Hoel, S. Xie, C. Benmore, C. D. Malliakas, J.-F. Gaillard, and K. R. Poeppelmeier, Z. Anorg. Allg. Chem. **637**, 885 (2011).